Molecular Dynamics Simulations of Small Halogenated Organics at the Air–Water Interface: Implications in Water Treatment and Atmospheric Chemistry

ARTICLE *in* THE JOURNAL OF PHYSICAL CHEMISTRY A · AUGUST 2013

Impact Factor: 2.69 · DOI: 10.1021/jp405292k · Source: PubMed

3 AUTHORS:

Alena Habartova
Academy of Sciences of the Czech Republic
8 PUBLICATIONS **12** CITATIONS
SEE PROFILE

Kalliat Valsaraj
Louisiana State University
232 PUBLICATIONS **3,641** CITATIONS
SEE PROFILE

Martina Roeselova
Academy of Sciences of the Czech Republic
46 PUBLICATIONS **893** CITATIONS
SEE PROFILE

THE JOURNAL OF PHYSICAL CHEMISTRY A

Article

pubs.acs.org/JPCA

Molecular Dynamics Simulations of Small Halogenated Organics at the Air−Water Interface: Implications in Water Treatment and Atmospheric Chemistry

Alena Habartová,[†] Kalliat T. Valsaraj,*[,‡] and Martina Roeselová*[,†]

[†]Institute of Organic Chemistry and Biochemistry, Academy of Sciences of the Czech Republic, Flemingovo nám. 2, 16610 Prague 6, Czech Republic

[‡]Cain Department of Chemical Engineering, Louisiana State University, Baton Rouge, Louisiana 70803, United States

Supporting Information

ABSTRACT: Free energy profiles associated with transfer of chlorinated and brominated halomethane molecules from the gas phase across the water−vapor interface to the aqueous phase were calculated using classical molecular dynamics simulations. The investigated species include chloromethane (CH_3Cl), bromomethane (CH_3Br), dichloromethane (CH_2Cl_2), dibromomethane (CH_2Br_2), chloroform ($CHCl_3$), and bromoform ($CHBr_3$). The employed halomethane force field was tuned by scaling up the atomic charges to reproduce the experimental hydration free energies. The computed free energy profiles have a minimum at the water−vapor interface of about 12−15 kJ·mol^{-1} relative to full hydration in the bulk liquid. This implies that the halomethanes exhibit enhanced interfacial concentrations in systems with large surface area per unit volume, such as air bubbles dispersed in water or water droplets dispersed in air. Implications for water treatment as well as for atmospheric chemistry are discussed.

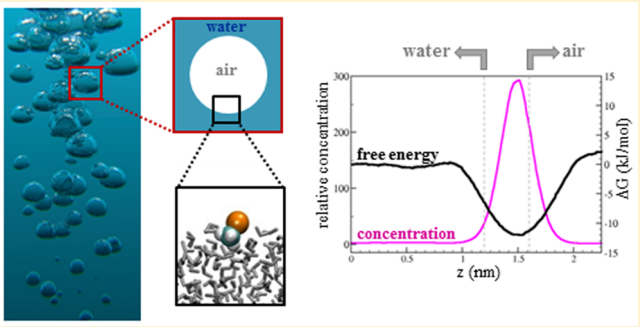

1. INTRODUCTION

Haloalkanes are a group of organic compounds derived from alkanes and containing one or more halogen substituents. They are prevalent pollutants in waste waters, groundwater, and in the atmosphere.[1,2] This results from their widespread use in industrial and agricultural operations as excellent solvents, flame retardants, and fumigants. Leaking valves and fugitive emissions are among the sources of these pollutants. Low molecular weight chlorinated haloalkanes are also formed in drinking water during treatment such as disinfection. A number of separation processes are used to remediate the water environment. These include the use of air stripping, activated carbon, and other adsorbent media.[3] Air stripping includes conventional bubble aeration and packed tower stripping, both of which are economically feasible. Adsorbent use for removing pollutants requires regeneration or proper disposal of the adsorbent after use.

Most of air stripping process designs involve the use of air−water bulk phase relationships (Henry's constant) and the rate of mass transfer of pollutants between the bulk air and water phases. The efficiency of the process depends on increasing the air−water interfacial contact and this can be brought about by decreasing the bubble size in conventional bubble aeration.[4] It has, however, been known that for systems that involve very high surface area to volume ratios (such as minute air bubbles in water), surface adsorption mechanisms for pollutants should be considered in addition to bulk phase relationships.[5] One such process that made use of the air−water surface adsorption of pollutants is an adsorptive bubble separation process (bubble fractionation) called "solvent sublation".[6] In solvent sublation, very fine air bubbles remove pollutants by adsorption from the aqueous phase and the materials are stripped into an immiscible organic solvent floated on top of the aqueous phase.[7,8] The process has been found to be very successful in removing a variety of organic pollutants such as chlorinated organics, aromatic hydrocarbons, and pesticides. Solvent sublation has been extensively tested on the laboratory scale and further tested on a pilot-scale as well on the industrial scale.[9−14] The success of solvent sublation in removing organic hydrophobic compounds was proven to be as a result of the air−water interface having the capability to transport volatile, semivolatile, and nonvolatile compounds from the aqueous phase.

The inverse problem arises in the atmosphere for water droplets scavenging organic compounds from the gas phase, which is termed "wet deposition" by rain, fog, dew, and mist. This process is important for atmospheric aerosols that affect both climate change and atmospheric chemistry. In this context, understanding the heterogeneous processes that occur on the

Received: May 29, 2013
Revised: August 22, 2013
Published: August 26, 2013

   dx.doi.org/10.1021/jp405292k | J. Phys. Chem. A 2013, 117, 9205−9215

surfaces of atmospheric dispersoids (cloud droplets, fog droplets, dew, and mist) becomes significant. Hence, for wastewater treatment and atmospheric wet deposition the essential element is the presence of one phase dispersed (as bubbles or drops) in another bulk phase to affect mass transfer and reaction at the interface between the two phases.

Although a number of experimental and correlation data on the air−water interfacial adsorption is available in the literature,[15−20] theoretical work has only recently begun to explore the adsorption phenomena at the air−water interface for natural surfactants[21−24] as well as for small organic molecules that are traditionally not called "surface-active".[25−27] Molecular dynamics simulation work has shown that a number of molecules including oxidants have the propensity for the air−water interface since they display substantial free energy minima at this interface.[21,25,26,28−31] Most of these computational studies have been performed on larger aromatic compounds such as polycyclic aromatic hydrocarbons (PAHs). Halogenated organics at the air−water interface have received little attention up to this point. Recent classical and ab initio MD simulation studies[32,33] of several monosubstituted haloalkanes showed their strong preference for interfacial solvation rather than full solvation in bulk liquid water even for the smallest and most water-soluble of these compounds, methyl chloride (CH_3Cl) and bromide (CH_3Br). It is important to investigate the free energy profiles at the air−water interface for halogenated organics so that their equilibrium and reaction rates at the interface can be better understood. This will help in not only improving the design of separation processes but also in understanding how water droplets in air can support reactions leading to atmospheric processing by clouds and fogs.[34]

This paper reports molecular dynamics investigation of a series of chlorinated and brominated halomethane species, including chloromethane (CH_3Cl), bromomethane (CH_3Br), dichloromethane (CH_2Cl_2), dibromomethane (CH_2Br_2), chloroform ($CHCl_3$), and bromoform ($CHBr_3$). For each compound, we have obtained the free energy profile associated with moving the molecule from the gas phase across the water−vapor interface to the aqueous phase. Our calculations are compared to the available experimental free energies of hydration derived from measured Henry's law constants,[35] and the computed free energy profiles are used to elucidate the interfacial partitioning of the halomethane species. Implications of our observations for water remediation using the air stripping method as well as potential impacts on atmospheric chemistry of halogenated organics are discussed.

An important contribution of the paper is the force field for interaction of halomethanes with water, which was tuned to the experimental free energy of hydration of each compound (obtained from Henry's law constants) via scaling of the atomic charges. This force field, albeit simple and nonpolarizable, is shown to provide quantitative results for the present set of halomethane compounds at the water−vapor interface, and is expected to be reliable when used in more complex MD simulations involving halomethanes.

2. METHODOLOGY

2.1. Computational Approach. Classical molecular dynamics (MD) simulations were used to investigate the aqueous hydration and surface propensity of the following set of halomethane molecules: CH_3Cl, CH_2Cl_2, $CHCl_3$, CH_3Br, CH_2Br_2, and $CHBr_3$. The simulated systems consisted of one halomethane molecule from the above list and 863 water molecules forming a slab of liquid with two water−vapor interfaces. The water slab was placed in the middle of a rectangular parallelepiped simulation box, with the *x*-, *y*-, and *z*-dimension of 3.0, 3.0, and 10.0 nm, respectively. The *z*-axis coincides with the direction normal to the two water−vapor interfaces. The thickness of the liquid water slab was approximately 3 nm. Periodic boundary conditions were applied in all three dimensions. This setup was utilized to evaluate the free energy profile associated with moving each halomethane molecule along the *z*-axis from the gas phase across the water−vapor interface into the bulk liquid, and then across the other water−vapor interface back into the gas phase. The simulation setup is shown in Figure 1a, and a schematic free energy profile of a halomethane molecule along the *z*-axis is depicted in Figure 1b.

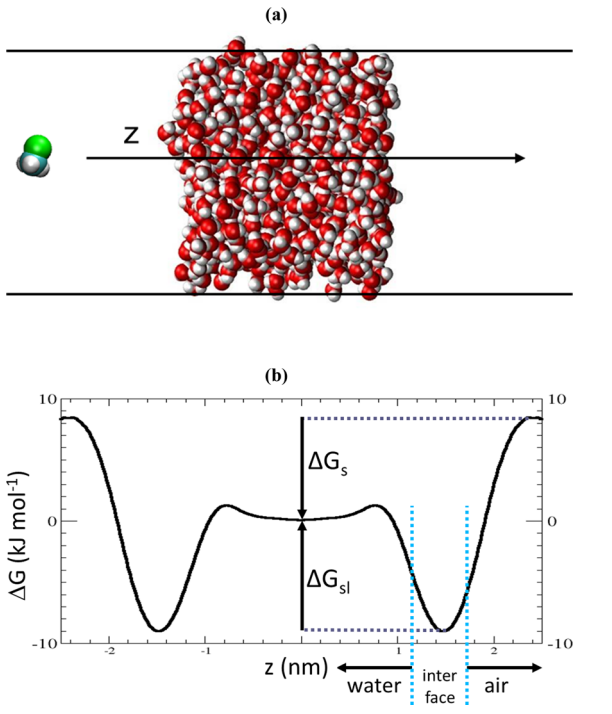

Figure 1. (a) Schematic depiction of the free energy profile coordinate across a liquid water slab. (b) Typical free energy profile of a haloalkane molecule.

As the molecule moves from the gas phase toward the bulk liquid water, its free energy goes through a minimum at the water−vapor interface, then increases again, and finally reaches a plateau in the interior of the water slab. The free energy difference of the transition of the solute from the gas to the liquid phase, ΔG_s, represents the free energy of hydration of the given species, and ΔG_{sl} is the free energy of the transition from the water surface into the bulk liquid. We note that the ΔG profile corresponds to the limit of infinite dilution. The experimental hydration free energy, ΔG_s^0, corresponding to the standard state of p_0 = 1 atm gas pressure and c_0 = 1 mol·L^{-1} aqueous concentration differs from the ΔG_s value pertinent to the present simulations with a single solute molecule by a constant according to[31,35]

$$\Delta G_s = \Delta G_s^0 + RT\left(\frac{p_0}{c_0 RT}\right) = \Delta G_s^0 - 7.9\ \text{kJ·mol}^{-1} \quad (1)$$

dx.doi.org/10.1021/jp405292k | J. Phys. Chem. A 2013, 117, 9205−9215

Table 1. Henry's Law Constant (k_H) and the Corresponding Experimental Free Energy of Hydration (ΔG_s^H), Calculated Free Energy of Hydration (ΔG_s), Interfacial Free Energy Minimum (ΔG_{sl}) Relative to the Liquid Phase, and the Relative Aqueous and Interfacial Concentrations with Respect to the Gas Phase As Obtained from the Calculated Free Energy Profiles for the Set of Halomethanes Studied[a]

	k_H	ΔG_s^H	ΔG_s	ΔG_{sl}	relative concentration			
molecule	(M/atm)	(kJ·mol^{-1})	(kJ·mol^{-1})	(kJ·mol^{-1})	gas phase	aqueous bulk	surface (maximum)	surface (averaged)
CH_3Cl	0.10	−2.2	−2	12	1	2	300	200
CH_2Cl_2	0.40	−5.6	−6	11	1	9	900	600
$CHCl_3$	0.25	−4.5	−4	12	1	6	800	500
CH_3Br	0.16	−3.4	−4	11	1	4	400	300
CH_2Br_2	1.10	−8.1	−6	15	1	26	8700	5600
$CHBr_3$	1.90	−9.5	−11	12	1	45	6500	5100

[a]For the interfacial concentration, both the maximum and averaged values are shown (see text for details). ΔG is set to 0 in the aqueous phase. For definition of ΔG_s and ΔG_{sl} see Figure 1b.

where R is the universal gas constant and T stands for temperature (T = 298.15 K for the standard state). The experimental free energy of hydration, ΔG_s^0, can be obtained from the Henry's law constant, k_H, using the following relation[35]

$$\Delta G_s^0 = -RT \ln\left(\frac{p_0}{c_0} k_H\right) \quad (2)$$

The Henry's law constant, k_H, in the above equation is defined as the equilibrium ratio of the molar concentration of a compound in the aqueous phase and its partial pressure above the liquid and is expressed in the units of M·atm^{-1}. Equation 1 is used to compare the MD-computed free energies of hydration with the experimental ones and to verify the quality of the employed force fields.

In addition, the free energy difference ΔG_{12} between any two points 1 and 2 selected along the free energy path can be used to evaluate the molar concentration ratio of the given species at these points

$$\frac{c_1}{c_2} = \exp\left(-\frac{\Delta G_{12}}{RT}\right) \quad (3)$$

Specifically, by setting the reference point 1 into the gas phase and selecting point 2 in the aqueous phase or at the liquid−vapor interface, one can use the corresponding ΔG values, namely ΔG(gas→liquid) = ΔG_s and ΔG(gas→interface) = $\Delta G_s - \Delta G_{sl}$, to calculate the partitioning of a species between the gas phase, the aqueous phase, and the liquid−vapor interface.

2.2. Computational Details and Potential Parameters. The free energy profiles were computed from a set of umbrella sampling simulations.[36−38] A single halomethane molecule was introduced into the gas phase region of the simulation box containing a pre-equilibrated liquid water slab, approximately 1.0 nm away from the water surface. First, a 4 ns constant volume and temperature (NVT) simulation was performed in which the center of mass (CoM) of the halomethane molecule was pulled along the z-direction (normal to the interface) toward the center of the water slab and then across the opposite interface into the gas phase using a harmonic restraining potential with the force constant of 1000 kJ·mol^{-1}·nm^{-2} and a pull rate of 0.002 nm·ps^{-1}. From this simulation, 60 configurations ("windows") with different positions of the halomethane molecule along the z-axis were extracted. Two different widths of the windows were employed: The first 10 and the last 10 windows (i.e., the windows located in the gas phase within −2.5 nm ≤ z ≤ −2.0 nm and 2.0 nm ≤ z ≤ 2.5 nm) were spaced by 0.05 nm, the remaining 40 windows within −2.0 nm ≤ z ≤ 2.0 nm were spaced by 0.1 nm. The finer spacing of the outermost windows was chosen in order to increase the precision of the ΔG calculation in the gas phase region far away from the water surface where the force exerted on the solute molecule by the water slab is subject to large fluctuations. For each of the 60 windows, a separate 6 ns NVT simulation was then carried out in which a biasing harmonic potential with the force constant of 3000 kJ·mol^{-1}·nm^{-2} was applied to the halomethane CoM. From the instantaneous values of the z-coordinate of the halomethane CoM, collected at 4 ps intervals, the umbrella sampling population histograms were constructed for the individual windows. Finally, the free energy profile was obtained from the umbrella sampling histograms using the weighted histogram analysis method (WHAM).[39,40] The MD simulations were carried out by the GROMACS 4.5.1[41] molecular dynamics package; the Gromacs utility g_wham[38] was utilized to perform the WHAM calculation and to estimate the statistical errors along the free energy profile with the bootstrapping analysis. A total of 100 bootstrap cycles were used.

The TIP4P-2005 force field[42] was used for water. This force field is currently one of the most universal water models that provides good description of water phase diagram over a wide range of temperatures and pressures.[43,44] The general Amber force field (GAFF)[45] was employed for the halomethanes. The Lennard-Jones parameters for the C, H, Cl, and Br centers are given in the Supporting Information, Table S1. The atomic partial charges were evaluated from molecular structures optimized at the B3LYP/cc-pVTZ level by the restrained electrostatic potential (RESP) method, fitting the electrostatic potential generated by the molecular charge distribution at points selected according to the Merz−Singh−Kollman scheme.[46] The ab initio calculations were conducted using Gaussian09 package,[47] the RESP calculations were performed by Antechamber.[48] The force fields employed in our MD simulations are nonpolarizable, that is, the model does not explicitly include the description of electronic polarization. However, polarization effects are implicitly taken into account in the interaction potentials. First of all, the parametrization of the TIP4P/2005 water model includes an average increase of the molecular dipole moment relative to its gas phase value due to polarization forces experienced by a water molecule in the condensed phase. In a similar way, the increase of the atomic partial charges of the halomethane molecules relative to their gas-phase values accounts for the average polarization effects of

dx.doi.org/10.1021/jp405292k | J. Phys. Chem. A 2013, 117, 9205−9215

the aqueous environment. The atomic charges of the halomethane molecules evaluated by the RESP procedure, the charge scaling factors and the atomic charges after scaling are given in the Supporting Information, Table S2. An individual charge scaling factor was chosen for each of the halomethane species so as to yield a good agreement with the experimental hydration free energy, as obtained from the available Henry's law constants. The values of the Henry's law constants used in this study (see Table 1) were obtained as an average of the Henry's law constant values reported by different authors as summarized in the compilation by Sander.[35] With the exception of one or two outliers, the range of the experimental Henry's law constant values corresponds to an uncertainty in the free energy of hydration (ΔG_s^H, see Table 1), which is comparable to the ± 2 kJ·mol^{-1} error of our free energy calculation.

All MD simulations were performed in an NVT ensemble at T = 300 K using the leapfrog integrator[49] with a time step of 1 fs. The system temperature was controlled by the v-rescale thermostat (temperature coupling using velocity rescaling with a stochastic term)[50] with a coupling time of 1 ps. The cutoff distance of 1.0 nm was employed for the Lennard-Jones and the short-range part of the Coulomb interactions. The neighbor list was updated every 10 integration steps. The long-range part of the Coulomb interaction was evaluated using the Particle-Mesh Ewald method[51,52] with a relative tolerance of 10^{-5}, fourth order cubic interpolation and a Fourier spacing parameter of 0.12. All bonds were constrained using LINCS.[53]

3. RESULTS

3.1. Free Energy Profiles and Interfacial Concentrations. The calculated free energy profiles of the set of chlorinated and brominated halomethane molecules (CH_3Cl, CH_2Cl_2, $CHCl_3$, CH_3Br, CH_2Br_2, and $CHBr_3$) are displayed in Figure 2. While the free energy profiles were calculated by moving each molecule from the gas phase through the entire water slab back into the gas phase at the opposite side of the slab, only the profiles for $z > 0$ are shown (with $z = 0$ corresponding to the middle of the water slab). They were obtained by averaging the computed ΔG values over the two equivalent half-spaces in the simulation system. The original free energy curves for both halves of the aqueous slab are available in the Supporting Information (Figure S1). They provide proof that the free energy profiles computed across the water slab (i.e., before averaging) were sufficiently symmetric. The deviations from perfect symmetry across the two equivalent water−vapor interfaces can serve as a measure of uncertainty of the computed ΔG values and of the convergence of the umbrella sampling calculations. The largest deviation observed is ± 2 kJ·mol^{-1}. Another way to estimate the statistical error is using the bootstrapping analysis (see Section 2.2. above). The free energy profiles from Figure 2 including the error bars computed by the bootstrapping technique are shown in Figure S2 of the Supporting Information. The largest error obtained by this approach is ± 1 kJ·mol^{-1}. The ΔG uncertainties of the order of 1−2 kJ·mol^{-1} are comparable with the errors reported in similar calculations for other small organic molecules at the water−vapor interface.[54]

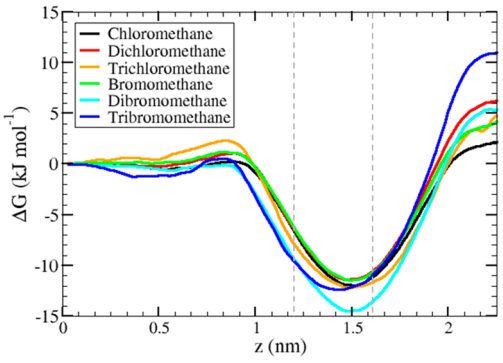

Figure 2. Computed free energy profiles of the chlorinated and brominated halomethanes across the liquid−vapor interface. The z-coordinate values represent the CoM of chloromethane. The z-axis lies in the direction normal to the liquid−vapor interface, z = 0 corresponds to the center of the water slab. The two vertical dashed lines denote the interfacial water layer.

The free energy difference between the gas phase and bulk liquid corresponds to the hydration free energy, ΔG_s. As discussed above, the hydration free energy can be obtained from the experimentally measured Henry's law constant. Thus, reproducing the ΔG_s value in a simulation helps to properly set the parameters of the molecular model. The comparison between the experimental hydration free energies (as obtained from the respective Henry's law constants) and the MD-calculated values is given in Table 1 and shows a good agreement. This was achieved by increasing the atomic partial charges of the halomethane molecules in order to account on average for the polarization effects due to the aqueous environment. The charge scaling factors needed to reproduce the free energy of hydration of the individual halomethane species range between 1.7 and 2.0 (see Supporting Information, Table S2).

For all of the halomethanes studied, the free energy profiles in Figure 2 exhibit a minimum in the liquid−vapor interfacial region corresponding to ΔG_{sl} of 12−15 kJ·mol^{-1} (ΔG_{sl} is defined as the free energy of the transition from the water surface into the bulk liquid, see Figure 1b). The ΔG_{sl} values for the individual compounds are given in Table 1. Unlike the free energy of hydration, which can be obtained from experimental measurements, the depth of the interfacial free energy minimum is experimentally very difficult to access. MD simulations thus provide an invaluable insight into the interfacial behavior of the halomethane species. Results of any classical MD simulation, however, depend critically on the quality of the underlying model. In the present case, as specified above in Section 3, the halomethane force field parametrization is a combination of the standard GAFF[55] parameters and ab initio/RESP-calculated atomic partial charges, which were uniformly increased by applying a scaling factor. For each halomethane species, free energy profile calculations were performed using several different scaling factors; the final results shown in Figure 2 and Table 1 were obtained with the atomic charges that reproduced best the experimental free energies of hydration. The free energy profiles calculated with different values of the charge scaling factor (see Supporting Information, Figure S3) can be used to assess the sensitivity of the results with respect to the charge distribution of each halomethane compound. Our results show that the computed free energy of hydration, ΔG_s, is highly sensitive to the charge scaling factor: ΔG_s values typically range between -10 kJ·mol^{-1} and $+10$ kJ·mol^{-1} for the charge scaling factor between 1.0 and 2.0. However, regardless of the scaling factor, the interfacial free energy minimum is always present and its depth (relative to the bulk liquid) is rather independent of the atomic charges. In the

dx.doi.org/10.1021/jp405292k | J. Phys. Chem. A 2013, 117, 9205−9215

majority of cases, the ΔG_{sl} values obtained with the scaling factor between 1.0 and 2.0 fall within or only slightly beyond the 4 kJ·mol^{-1} interval corresponding to the ±2 kJ·mol^{-1} uncertainty in the free energy calculation. Therefore, we conclude that the present MD simulations provide robust results as regards the free energy minimum of halomethane molecules at the water−vapor interface. Similar, albeit less deep interfacial free energy minima ($\Delta G_{sl} \approx 2-6$ kJ·mol^{-1}) have been reported for a set of atmospheric gases (N_2, O_2, O_3, OH, H_2O, HO_2, and H_2O_2).[28,30,31] The depths of the interfacial free energy minima of the halomethanes, as yielded by the present calculations ($\Delta G_{sl} \approx 12-15$ kJ·mol^{-1}), reflects the stronger attractive interaction between the halogenated compounds and water surface compared to the above gas molecules and radicals. The ΔG_{sl} values obtained for halomethanes are comparable to those predicted for benzene and small polycyclic aromatic hydrocarbons.[25,26] Similar free energy minima, ranging between 6 kJ·mol^{-1} for methanol and 28 kJ·mol^{-1} for neopentane, were also found for a set of small organic molecules of varying degree of hydrophobicity at the surface of water droplets.[54]

A recently published thermodynamic analysis[54] demonstrated that the preference of organic molecules to be partially solvated at the water−vapor interface rather than inside the bulk liquid is primarily an enthalpic effect, which is modulated by entropy. For molecules containing large nonpolar groups, however, the entropic component becomes significant, resulting in further enhancement of the magnitude of surface preference due to the hydrophobic effect. Following the previous studies of solutes at the surface of water droplets[54,56] and infinite water slab,[21] we have attempted to decompose the free energy profiles $\Delta G(z)$ into the enthalpic component $\Delta H(z)$ and the entropic component $-T\Delta S(z)$. The enthalpic component was determined as the average potential energy of the system over the simulation in each of the umbrella sampling windows along the z-coordinate. The average potential energy of the system was computed as the average of the sum of the respective Lennard-Jones and Coulomb interactions. The entropic component was calculated as the difference between the free energy profile and the enthalpic contribution at a given value of the z-coordinate: $-T\Delta S(z) = \Delta G(z) - \Delta H(z)$. The results are shown in the Supporting Information, Figure S4. Qualitatively, the overall character of the $\Delta H(z)$ and $-T\Delta S(z)$ curves agrees with what has been reported in the previous studies:[21,54,56] The enthalpic curves tend to exhibit a minimum at the interface, indicating that the solutes are stabilized in the interfacial region mainly due to the energy interactions with the water molecules. At the same time, the entropic components $-T\Delta S$ tend to increase as the solutes move from the gas phase across the interface into the bulk liquid phase. We wish to stress, however, that in contrast to the previous work on organic solutes at the surface of small water droplets[54] both the enthalpic and entropic contributions in the present case are subject to very large uncertainty due to large fluctuations of the system's potential energy with a standard deviation of ±200 kJ·mol^{-1} (see Figure S5, Supporting Information). This uncertainty is significantly greater than the range of changes of $\Delta H(z)$ or $-T\Delta S$ across the entire interfacial system. Thus, in the present case of halomethanes at the extended water−vapor interface, the attempt to split the free energy profiles into their enthalpic and entropic components does not yield meaningful results.

From the free energy profile, $\Delta G(z)$, along the z-coordinate normal to the two liquid−vapor interfaces of the water slab, one can evaluate the corresponding relative concentration profile $c_{rel}(z)$ of the halomethane species across the liquid bulk/interface/gas phase system. Equation 3, upon setting the reference point into the gas phase, can be rewritten in terms of the concentration profile relative to the gas phase concentration, c_g, as

$$c_{rel}(z) = \frac{c(z)}{c_g} = \exp\left(-\frac{\Delta G(z) - \Delta G_s}{RT}\right) \quad (4)$$

As an example, the free energy profile and the corresponding concentration profile for chloromethane is shown in Figure 3.

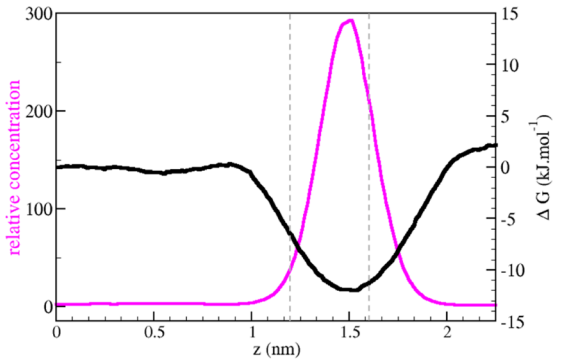

Figure 3. Free energy profile (black line) and the corresponding concentration profile (purple line) of chloromethane across the water−vapor interface. The concentration profile is calculated using eq 4 relative to the gas phase concentration ($c_{rel} = 1$ in the gas phase). The z-coordinate values represent the CoM of chloromethane. The z-axis lies in the direction normal to the liquid−vapor interface, $z = 0$ corresponds to the center of the water slab. The two vertical dashed lines denote the interfacial water layer.

The free energy minimum at the liquid−vapor interface gives rise to a substantial enhancement of chloromethane concentration in the interfacial region with respect to both the gas phase and liquid phase concentrations. Similar results were obtained for all of the halomethane species under investigation. The results are summarized in Table 1, which shows for each of the species studied their aqueous bulk concentrations (relative to the gas phase) and the maximum relative concentrations at the water−vapor interface (corresponding to the point of the free energy minimum). In addition, the relative concentrations averaged over the entire interfacial layer are reported. For the purpose of the integration, the liquid−vapor interface is defined as the region between the z-coordinate values z_{90} and z_{10} for which the water density reaches 90% and 10% of its bulk liquid value, respectively. For our slab system, $|z_{90}| = 1.23$ nm and $|z_{10}| = 1.62$ nm with $z = 0$ in the middle of the water slab. The averaged interfacial concentrations are likely to reflect more realistically the situation at the dynamic liquid−vapor interface. Albeit lower than the maximum values, the averaged values still imply enhanced surface concentrations by 2−3 orders of magnitude compared to the gas phase, and an appreciable surface enhancement with respect to the aqueous phase concentration ranging from a factor of ∼70 to ∼200, depending on the halomethane species.

The significant surface enhancement, indicating a strong preference for interfacial solvation, has been previously predicted for two of the present molecules (chloromethane and bromomethane) from unconstrained classical MD trajectories that sampled the time development of the

dx.doi.org/10.1021/jp405292k | J. Phys. Chem. A 2013, 117, 9205−9215

molecular position along the direction normal to the water−vapor interface of liquid water slab.[32] For chloromethane, a similar result was obtained by ab initio (DFTB-D) molecular dynamics simulations.[33] The position distribution (density profile) obtained from such direct sampling should in principle agree with the concentration profile computed from the free energy profile (Figure 3). In this particular case, however, the comparison is not straightforward, because the sampling trajectories of ref 32 and the present free energy calculations were each based on a different interaction model. While in both cases the GAFF parameters were used for CH_3Cl and CH_3Br, the former MD simulations utilized a polarizable CH_3Cl/CH_3Br model with unscaled RESP charges based on an MP2/cc-pvdz calculation combined with polarizable POL3 water force field, whereas the free energy profiles in this work were computed using a nonpolarizable model for CH_3Cl/CH_3Br with scaled atomic charges (RESP charges based on an B3LYP/cc-pvtz calculation enlarged by a factor of 1.7 for CH_3Cl and 1.95 for CH_3Br) and nonpolarizable TIP4P-2005 water force field.

To enable direct comparison between the two methods of computing the concentration profile across the water−vapor interface (direct sampling vs free energy profile calculation), we performed a 100 ns MD simulation of chloromethane and bromomethane interacting with the water slab using the present (nonpolarizable) model. The simulated system and computational details were the same as in the free energy profile calculations (see Sections 2.1 and 2.2), except that two (instead of one) CH_3Cl or CH_3Br molecules in the simulation box were used to enhance the sampling efficiency. The resulting CH_3Cl trajectories are available in the Supporting Information, Figure S6. The corresponding position distribution of chloromethane along the z-coordinate, equivalent to the concentration (or number density) profile across the water−vapor interface, is shown in Figure 4 (green line) together with the concentration profiles obtained from the present free energy profile calculation (purple line) and from the previous simulation with a polarizable force field[32] (blue line). All concentration profiles are normalized relative to the gas phase concentration (i.e., c_{rel} = 1 in the gas phase). Similar results were obtained for bromomethane (not shown). The broadening of the interfacial concentration peaks obtained by direct sampling compared to the concentration profile derived from the free energy calculation (more pronounced for the longer nonpolarizable simulation than for the considerably shorter polarizable one) can be attributed to frequent evaporation of chloromethane from the water surface (see Figure S6 in the Supporting Information), which leads to a somewhat ill-defined center of mass of the water slab. Upon averaging over the trajectory, this results in an effective broadening of the interfacial layer. This effect is not present in the umbrella sampling simulations, in which the chloromethane position along the interfacial normal is restrained by the umbrella potential.

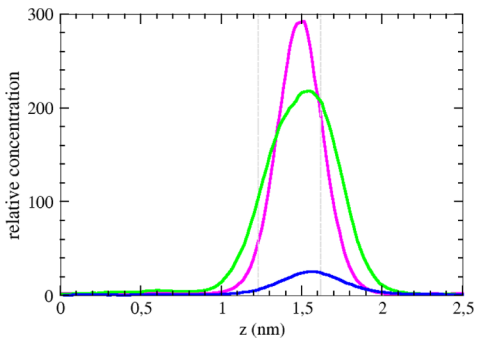

Figure 4. Concentration profiles of chloromethane across the water−vapor interface as obtained from the free energy profile calculation (purple line) and direct sampling simulations (green line) using the present nonpolarizable force field combined with the TIP4P-2005 water model. For comparison, results of previous simulation with a polarizable chloromethane force field in combination with POL3 water model are shown in blue. All concentration profiles are normalized relative to the gas phase concentration (c_{rel} = 1 in the gas phase). The z-axis lies in the direction normal to the liquid−vapor interface, z = 0 corresponds to the center of the water slab. The two vertical dashed lines denote the interfacial water layer.

As can be seen in Figure 4, the agreement of the concentration profile calculated for the present model by direct sampling with that derived from the free energy profile is rather satisfactory. In both cases, the region of the maximum concentration is located in the outer (vapor-side) layer of the interface, and both methods yield the enhancement of the interfacial concentration by 2 orders of magnitude with respect to the gas phase. The maximum relative interfacial concentration determined by direct sampling (c_{rel} = 220) agrees within the error bars with the value obtained from the free energy calculation (c_{rel} = 300 ± 170). On the other hand, the direct sampling predicts somewhat higher value (c_{rel} = 10) of the relative concentration in the bulk liquid than the free energy profile calculation (c_{rel} = 2 ± 1). The errors in c_{rel} were estimated based on the maximum uncertainty (±1 kJ·mol^{-1}) of the computed ΔG values obtained from the bootstrapping analysis (see above) using standard error propagation. The comparison with the previous MD simulation that employed the polarizable Amber force field is less favorable. While qualitatively similar, the predicted surface enhancement is an order of magnitude smaller than that obtained with the present nonpolarizable model. It is important to note that the results of the polarizable simulation are based on a significantly shorter sampling (20 ns trajectory) compared to the nonpolarizable simulation (100 ns trajectory). A more critical factor, however, is the fact that unlike the present nonpolarizable model the polarizable Amber force field used in ref 32 in combination with the POL3 water model was not optimized to reproduce the hydration free energy of the haloalkane species. In the light of the comparison with the results of the current study (Figure 4), it seems likely that the polarizable model[32] underestimates the strength of the haloalkane−water interactions and, therefore, also the magnitude of the haloalkane concentration enhancement at the aqueous surface. Thus, the present model, albeit based on a simpler, nonpolarizable force field with scaled charges, is nevertheless expected to provide more reliable results. Further work is needed to understand and quantify the role of polarization forces in the interfacial hydration of the haloalkane compounds and to refine the currently available polarizable force fields for MD simulations of haloalkanes in interfacial environments.

In summary, the computed free energy profiles indicate a significant propensity of single- and multisubsituted halomethanes to reside at the water−vapor interface. The present work thus corroborates the conclusions of previous MD simulation studies carried out for chloromethane (CH_3Cl)[32,33] and bromomethane (CH_3Br)[32] and provides a more quantitative picture regarding the interfacial hydration preferences of small halogenated organic species.

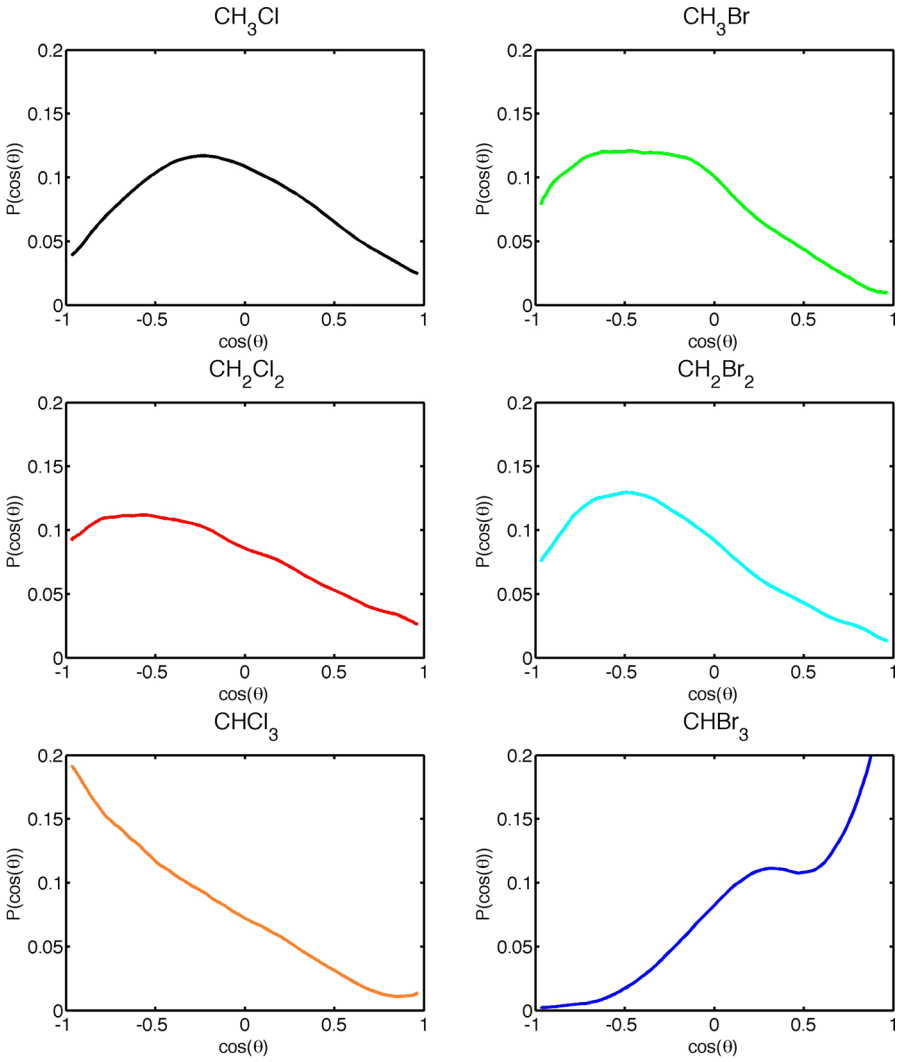

Figure 5. Orientation distributions of chlorinated and brominated halomethanes at the water−vapor interface. θ is the angle between the interface normal (z-axis) and the molecular vector $\vec{v}$, defined in the following way: (1) For the CH_3X species (upper two panels), the molecular vector points from the halogen atom X toward the carbon of the methyl group, $\vec{v}$ = X → C. (2) For the CH_2X_2 species (middle two panels), the molecular vector coincides with the bisector of the X−C−X angle and points toward the carbon atom. (3) For the CHX_3 species (bottom two panels), the molecular vector points from the carbon atom to the hydrogen, $\vec{v}$ = C → H.

3.2. Interfacial Orientation. The previous classical[32] and ab initio molecular dynamics simulations[33] showed that the surface-adsorbed chloromethane and bromomethane are (surprisingly) preferentially oriented with the methyl group toward the water. This has been rationalized on the basis of ab initio calculations in terms of the subtle balance of electrostatic, dispersion, induction, and hydrogen-bonded interactions. While in general the hydrogen bonds between alkyl halides and water are considered weak, in chloro- and bromomethane the large polarity of the C−H bonds of the methyl group immediately next to the halogen substituent makes the methyl group a preferential site for $CH_3\cdots OH_2$ hydrogen bonding. Indeed, ab initio calculations[33] showed that chloromethane primarily interacts with the water surface via the CH···O hydrogen bonds between the methyl group and water oxygen, whereas the OH···Cl hydrogen bonds between chlorine and water are weaker and less frequent. The empirical force field employed in the previous MD simulations[32] that included explicit treatment of polarization interactions was able to reproduce this behavior of chloromethane and bromomethane at the water−vapor interface.

In order to check the performance of the present force field as far as the preferential surface orientation of chloro- and bromomethane is concerned, we analyzed the 100 ns MD trajectories of two CH_3Cl or CH_3Br molecules interacting with a water slab in terms of the orientation distribution $P(\cos\theta)$, where θ is the angle between the interface normal (z-axis) and the molecular vector $\vec{v}$ = X → C pointing from the halogen atom X (= Cl or Br) to the carbon of the methyl group. In addition, we evaluated the $P(\cos\theta)$ distribution for chloromethane and bromomethane also from the respective umbrella sampling simulations in the z-coordinate window corresponding to the interfacial free energy minimum. Both approaches yielded practically the same results, therefore only the orientation distributions obtained from the umbrella sampling simulations are shown in Figure 5 (upper two panels). For the molecular vector $\vec{v}$ = X → C, $\cos\theta = 0$ means that the CH_3X molecule is aligned with the molecular axis parallel to the surface, $\cos\theta = 1$ corresponds to the molecular axis oriented perpendicular to the surface with the methyl group pointing to the gas phase, whereas $\cos\theta = -1$ denotes a perpendicular orientation of the molecular axis relative to the surface with the

dx.doi.org/10.1021/jp405292k | J. Phys. Chem. A 2013, 117, 9205−9215

methyl group facing toward water. The $P(\cos\theta)$ distributions of chloromethane and bromomethane show that molecular orientations parallel to the interface as well as tilted orientations with the methyl group pointing toward water are preferred (see the snapshots in upper two panels of Figure 6), whereas the

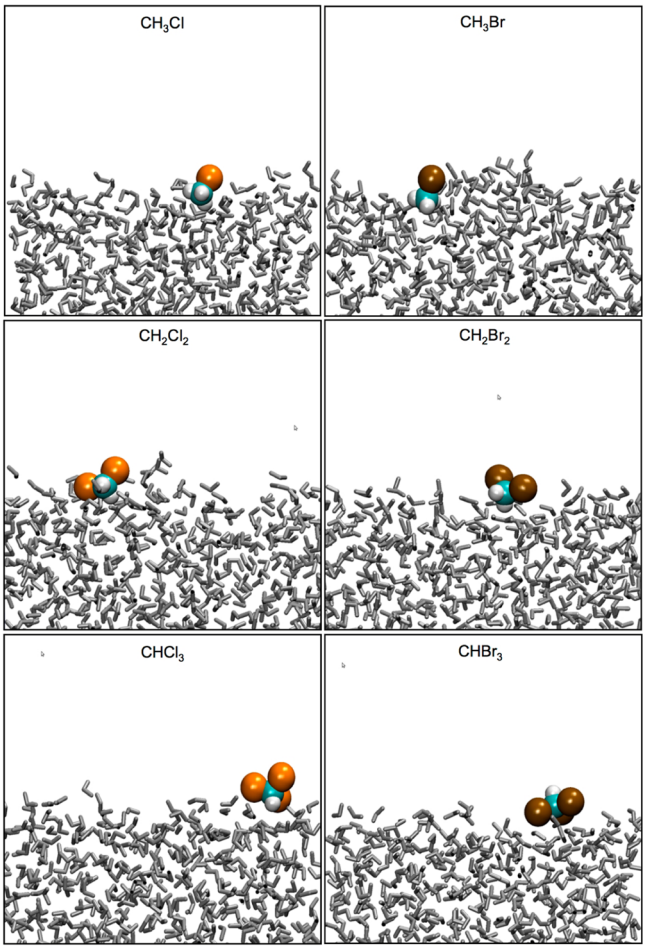

Figure 6. Example of snapshots showing the preferential orientation of chloro- and bromomethanes at the water−vapor interface.

orientations with the halogen atom facing the water surface are disfavored. This is consistent with the results of the previous MD studies of CH_3Cl and CH_3Br at the water−vapor interface[32,33] and demonstrates that the present nonpolarizable force field is able to represent reliably the preferential orientation of chloro- and bromomethane in the aqueous interfacial layer, observed in the earlier simulations that employed more sophisticated description of the interaction potential, either at the ab initio (DFTB-D) level (cf. Figure 7 of ref 33) or at the empirical force field level with polarization interaction explicitly included (see Figure 6 of ref 32).

It would be of interest to know the preferred interfacial orientation also for the other halomethanes investigated here. To this end, we calculated their orientation distributions from the respective umbrella sampling simulations in the z-coordinate window corresponding to the interfacial free energy minimum of each compound. For dichloro- and dibromomethane (CH_2X_2, middle two panels of Figure 5) the molecular vector $\vec{v}$ coincides with the bisector of the X−C−X angle and points toward the carbon atom. Thus, $\cos\theta = 1$ corresponds to the molecular vector oriented perpendicular to the surface with the halogen atoms pointing toward water and the hydrogen atoms toward the vapor phase, whereas $\cos\theta = -1$ means a perpendicular orientation of the molecular vector relative to the surface with the hydrogen atoms facing toward water and the halogen atoms toward the vapor phase. For $\cos\theta = 0$, the molecular vector of CH_2X_2 is aligned parallel to the surface. As can be seen from the distributions, dichloro- and dibromomethane exhibit orientation behavior similar to chloro- and bromomethane. The configurations with the hydrogen atoms facing toward water are preferred over the configurations with the hydrogen atoms pointing away from water, into the gas phase (typical snapshots are shown in Figure 6). For trichloro- and tribromomethane (CHX_3, bottom two panels of Figure 5), the molecular vector points from the carbon atom to the hydrogen, $\vec{v}$ = C → H. Once again, for this definition $\cos\theta = 1$ corresponds to the molecular vector of CHX_3 oriented perpendicular to the surface with the hydrogen atoms pointing toward the vapor phase, whereas $\cos\theta = -1$ represents a perpendicular orientation of the molecular vector relative to the surface with the hydrogen atoms facing toward water. The bottom left panel of Figure 5 shows that the latter configuration (i.e., with the hydrogen atom facing water) is strongly preferred for trichloromethane. However, a quite different behavior is seen for tribromomethane (bottom right panel, Figure 5). The distribution is bimodal with a secondary maximum corresponding to tilted orientation and the main maximum to perpendicular orientation of the molecular vector relative to the interface in both cases with the hydrogen atom of $CHBr_3$ pointing into the gas phase rather than toward water.

The dramatically different interfacial orientation of $CHBr_3$ compared to $CHCl_3$ (see Figure 6, bottom two panels) which falls outside the trends exhibited by the rest of the halomethane molecules studied may be an indication of the limitations of the present model. An ab initio study of trihalomethane−water complexes ($X_3CH\cdots OH_2$, X = F, Cl, Br, I) showed that all members of the trihalomethane series interact with the water molecule via the CH···O hydrogen bond.[57] Also the molecular electrostatic potential exhibits the same character for all trihalomethanes with the most positive region around the hydrogen atom.[58] On the other hand, the situation may be different for the halomethanes interacting with liquid water. The orientation of a molecule at the water surface is a result of the balance of hydrogen-bonding, electrostatic, induction, and dispersion interactions. This balance is particularly subtle for halomethanes since their hydrogen bonds with water are weak. Therefore, while the stabilization of the halomethane−water complexes comes predominantly from hydrogen-bonding, the dispersion, and induction terms may become comparable, or even dominant, at the water−vapor interface, especially for bromoform, with its three large and polarizable bromine atoms. This may result in a different orientation behavior of bromoform from the rest of the present halomethanes possessing either fewer or smaller and less polarizable halogen atoms. While it is possible to quantitatively reproduce the overall interaction of halomethanes with liquid water using an empirical force field, as demonstrated above by our free energy calculations, it is very difficult to represent all of the different contributions to the interaction energy reliably with such a simple model. More detailed study of the nature of the halomethane−water interaction, including a high-level ab initio investigation of larger halomethane−water complexes, is needed to rationalize the preferential surface orientations of di- and trihalomethanes observed in our MD simulations and to

dx.doi.org/10.1021/jp405292k | J. Phys. Chem. A 2013, 117, 9205−9215

test the adequacy of the model in this respect. Such study is, however, beyond the scope of the present paper.

To summarize, the nonpolarizable halomethane force field employed in this work reproduces well the preferential orientation of surface-adsorbed chloromethane and bromomethane with the methyl group toward water, predicted by a previous MD study with a polarizable force field[32] and subsequently confirmed by ab initio calculations.[33] Similar verification is necessary as far as the interfacial orientation of di- and trihalomethanes is concerned. We wish to emphasize, however, that even though the preferential surface orientation of some (or possibly all) of the multisubstituted halomethanes, as predicted by the present force field, may be incorrect, this does not affect the main result of this work, which is the significant concentration enhancement of all of the halomethanes at the water−vapor interface due to the existence of a pronounced interfacial free energy minimum. As shown by our present calculations (see Section 3.1 above and Figure S3 of the Supporting Information) as well as by an earlier work,[30] while the computed value of the free energy of hydration depends rather strongly on the choice of the force field, the calculated depth of the free energy minimum, and hence the magnitude of the concentration enhancement at the surface, is robust and much less sensitive to the underlying model and the particular choice of its parameters. Thus, although further refinement of the halomethane force field, which may be needed for correct description of the molecular orientation at the water surface, is likely to result in certain quantitative changes to the computed free energy profile and relative concentrations, we do not expect these changes to be of such an order as to significantly alter the overall picture obtained from the present study.

4. IMPLICATIONS FOR WATER TREATMENT AND ATMOSPHERIC CHEMISTRY

As stated in the introduction, the air−water interface plays a dominant role in two areas: (a) the use of bubble fractionation or aeration (air bubbles dispersed in water) for treatment of dissolved haloalkanes, and (b) in wet deposition scavenging of gaseous haloalkanes from air (water droplets dispersed in air). In both cases, the air−water interface area and the adsorption of haloalkanes at the interface will increase the overall efficiency of the process. The conventional partition constant (Henry's law constant) for bulk phase air−water relationship is insufficient to capture the process. Consider, for example, the case of water droplets dispersed in the atmosphere (as in cloud or fog) that contains a haloalkane compound in the gas phase. The uptake of the haloalkane into the droplet is determined by the partitioning between the air and the droplet phase. An effective Henry's constant (dimensionless molar ratio of aqueous to gas phase concentrations), K_H^* can be defined[5]

$$K_H^* = RTk_H + a_v K_{ia} \quad (5)$$

that accounts for both the conventional bulk water−air Henry's law constant, k_H/M·atm^{-1} (ratio of aqueous molar concentration in mol·L^{-1} to gas phase partial pressure in atm), and the interface−air adsorption constant, K_{ia}/cm (ratio of aqueous surface concentration in mol·cm^{-2} to molar gas phase concentration in mol·cm^{-3}). In the above equation, a_v is the surface area per unit volume of the dispersed phase. Note that although k_H remains constant, the effective Henry's constant K_H^* increases with the interface area and the partitioning to the air−water interface.

As the surface area per unit volume for the dispersed phase increases, the additional term that involves the surface area and interface partition constant has to be included. In the realm of bubble fractionation (and solvent sublation), the significance of the same has been shown via experimental and mathematical modeling of the bubble columns.[59−61] It has been shown that both mass transfer rate for the haloalkanes from water to air bubbles and the adsorption capacity of the air bubbles for haloalkanes increased with decreasing size of the air bubbles. In atmospheric chemistry, the behavior of haloalkanes toward wet deposition by dispersed droplets (aqueous aerosol, cloud droplets, fog, rain, and mist) and via adsorption on thin water films on solid surfaces (as well as on ice and snow) will also depend on the adsorption capacity at the air−water interface from air. The fact that the haloalkane compounds are preferentially partially hydrated at the surface will lead to their effective capture and transport from the air to water droplets. Techniques such as the sum frequency generation and other second order spectroscopic probes should provide support for the MD simulations, although the relatively weak haloalkane−water interaction compared to more traditional surface active species (e.g., alcohols), resulting in comparatively lower surface density and lower degree of orientation order, makes the detection of surface-adsorbed haloalkanes a challenging task for these methods, at least at ambient temperature.[32] It has also been shown that many atmospheric oxidants prefer the air−water interface.[28] Thus, the partial solvation phenomena of haloalkanes and atmospheric oxidants will potentially affect the heterogeneous oxidation reaction rates at the surface of aerosols and other dispersed droplets in contrast to fully solvated species within the aqueous phase.[62−64] In particular, it would be useful to further understand the reactivity of low molecular weight haloalkanes on thin films of water in ice and snow, as they are important from the perspective of ozone layer depletion in the Arctic and Antarctic regions.

5. CONCLUSIONS

Molecular dynamics simulations were used to calculate the free energy profiles of chlorinated and brominated halomethane molecules (CH_3Cl, CH_2Cl_2, $CHCl_3$, CH_3Br, CH_2Br_2, and $CHBr_3$) across the water−vapor interface. Our calculations reproduce well the experimental free energies of solvation derived from measured Henry's law constants. For all of the above halomethane species, the computed free energy profiles exhibit a minimum at the water−vapor interface of about 12−15 kJ·mol^{-1} relative to full hydration in the bulk liquid. This translates into enhanced interfacial concentrations by 2−3 orders of magnitude compared to the gas phase, and by a factor of ∼70 to ∼200 with respect to the aqueous phase concentration, depending on the particular halomethane. The present results indicate that small halogenated organics readily adsorb to aqueous surfaces and can accumulate in the water−vapor interfacial region. This has important implications for systems and processes in which the air−water interface plays a dominant role, for example, for air bubbles dispersed in water (such as in bubble aeration used in water treatment) or water droplets dispersed in air (wet deposition by aqueous aerosols, cloud droplets, fog, rain, and mist). The propensity of the haloalkane compounds for the water−vapor interface will lead to their effective transfer from water to air bubbles or, in the inverse case, to their capture and transport from the air to water droplets. The overall efficiency of the process will increase with increasing surface area of the dispersed phase per unit volume.

dx.doi.org/10.1021/jp405292k | J. Phys. Chem. A 2013, 117, 9205−9215

The fact that the low molecular weight haloalkanes are preferentially partially hydrated at the aqueous−air interfaces is of importance also for understanding heterogeneous chemical processes occurring at the surface of aerosols and other liquid droplets dispersed in air, on thin water films adsorbed on surfaces, or at the quasi-liquid layer on ice.

■ ASSOCIATED CONTENT

Supporting Information

Halomethane force field: Lennard-Jones parameters (Table S1), atomic charges and scaling factor values (Table S2). Unsymmetrized free energy profiles (Figure S1), free energy profiles with error bars computed by the bootstrapping technique (Figure S2), free energy profiles calculated using several different values of the scaling factor of atomic partial charges (Figure S3), decomposition of computed free energy profiles into enthalpic and entropic components (Figure S4), plot of the enthalpic components with a typical error bar shown (Figure S5), unconstrained trajectories of two chloromethane molecules interacting with a water slab (Figure S6). This material is available free of charge via the Internet at http://pubs.acs.org.

■ AUTHOR INFORMATION

Corresponding Authors

*E-mail: roesel@uochb.cas.cz (M.R.).
*E-mail: valsaraj@lsu.edu (K.T.V.).

Notes

The authors declare no competing financial interest.

■ ACKNOWLEDGMENTS

The authors wish to thank Robert Vácha, Ivan Gladich, Morteza Khabiri, Jana Hladílková, and Pavel Jungwirth for helpful discussions. The research was supported by the Czech Science Foundation (Grant 13-06181S) and by the funding to the Institute of Organic Chemistry and Biochemistry AS CR via RVO 61388963. Travel support to M.R. from the AirUCI Institute funded by the U.S. National Science Foundation (Grant 0909227) is also gratefully appreciated. K.T.V. acknowledges grants from the U.S. National Science Foundation (AGS 1106569) and the Gulf of Mexico Research Initiative (GoMRI) (LSU GRI Subaward TUL-629-11/12).

■ REFERENCES

(1) Symons, J. M.; Bellar, T. A.; Carswell, J. K.; DeMarco, J.; Kropp, K. L.; Robeck, G. G.; Seeger, D. R.; Slocum, C. J.; Smith, B. L.; Stevens, A. A. National Organics Reconnaissance Survey for Halogenated Organics. *J. Am. Water Works Assoc.* **1975**, *67*, 634.

(2) Finlayson-Pitts, B. J.; Pitts, J. N., Jr. *Chemistry of the Upper and Lower Atmosphere: Theory, Experiments, and Applications*; Academic Press: San Diego, 2000.

(3) Tchobanoglous, G.; Burton, F.; Stensel, H. D. *Metcalf & Eddy: Wastewater Engineering - Treatment and Reuse*; McGraw Hill Book Co.: New York, 2002.

(4) Eckenfelder, W. W., Jr. *Industrial Water Pollution Control*; McGraw-Hill: New York, 1966.

(5) Valsaraj, K. T. Adsorption of Polycyclic Aromatic Hydrocarbons at the Air-Water Interface and Its Role in Atmospheric Deposition by Fog Droplets. *Environ. Toxicol. Chem.* **2004**, *23*, 2318−2323.

(6) Karger, B. L. Solvent Sublation. In *Adsorptive Bubble Separation Techniques*; Lemlich, R., Ed.; Academic Press: New York, 1972.

(7) Valsaraj, K. T.; Thoma, G. J.; Thibodeaux, L. J.; Wilson, D. J. Studies in Batch and Continuous Solvent Sublation. 1. A Complete Model and Mechanisms of Sublation of Neutral and Ionic Species from Aqueous Solution. *Sep. Technol.* **1991**, *1*, 234−244.

(8) Clarke, A. N.; Wilson, D. J. *Foam Flotation: Theory and Applications*; Marcel Dekker: New York, 1983.

(9) Bryson, B. G.; Valsaraj, K. T. Solvent Sublation for Waste Minimization in a Process Water Stream - a Pilot-Scale Study. *J. Hazard. Mater.* **2001**, *82*, 65−75.

(10) Smith, J. S.; Valsaraj, K. T. The Promise of Solvent Sublation. *Chem. Eng. Progr.* **1998**, *94*, 69−76.

(11) Huang, S. D.; Valsaraj, K. T.; Wilson, D. J. Removal of Refractory Organics by Aeration. 5. Solvent Sublation of Naphthalene and Phenanthrene. *Sep. Sci. Technol.* **1983**, *18*, 941−968.

(12) Valsaraj, K. T.; Porter, J. L.; Liljenfeldt, E. K.; Springer, C. Solvent Sublation for the Removal of Hydrophobic Chlorinated Compounds from Aqueous-Solutions. *Water Res.* **1986**, *20*, 1161−1175.

(13) Valsaraj, K. T.; Wilson, D. J. Removal of Refractory Organics by Aeration. 4. Solvent Sublation of Chlorinated Organics and Nitrophenols. *Colloids Surf.* **1983**, *8*, 203−224.

(14) Lionel, T.; Wilson, D. J.; Pearson, D. E. Removal of Refractory Organics from Water by Aeration. 1. Methyl Chloroform. *Sep. Sci. Technol.* **1981**, *16*, 907−923.

(15) Valsaraj, K. T. On the Physicochemical Aspects of Partitioning of Non-Polar Hydrophobic Organics at the Air-Water-Interface. *Chemosphere* **1988**, *17*, 875−887.

(16) Hartkopf, A.; Karger, B. L. Study of Interfacial Properties of Water by Gas-Chromatography. *Acc. Chem. Res.* **1973**, *6*, 209−216.

(17) Roth, C. M.; Goss, K.-U.; Schwarzenbach, R. P. Adsorption of a Diverse Set of Organic Vapors on the Bulk Water Surface. *J. Colloid Interface Sci.* **2002**, *252*, 21−30.

(18) Kelly, C. P.; Cramer, C. J.; Truhlar, D. G. Predicting Adsorption Coefficients at Air−Water Interfaces Using Universal Solvation and Surface Area Models. *J. Phys. Chem. B* **2004**, *108*, 12882−12897.

(19) Goss, K.-U. Predicting Adsorption of Organic Chemicals at the Air-Water Interface. *J. Phys. Chem. A* **2009**, *113*, 12256−12259.

(20) Jubb, A. M.; Hua, W.; Allen, H. C. Organization of Water and Atmospherically Relevant Ions and Solutes: Vibrational Sum Frequency Spectroscopy at the Vapor/Liquid and Liquid/Solid Interfaces. *Acc. Chem. Res.* **2012**, *45*, 110−119.

(21) Liyana-Arachchi, T. P.; Stevens, C.; Hansel, A. K.; Ehrenhauser, F. S.; Valsaraj, K. T.; Hung, F. R. Molecular Simulations of Green Leaf Volatiles and Atmospheric Oxidants on Air/Water Interfaces. *Phys. Chem. Chem. Phys.* **2013**, *15*, 3583−3592.

(22) Hede, T.; Li, X.; Leck, C.; Tu, Y.; Ågren, H. Model Hulis Compounds in Nanoaerosol Clusters − Investigations of Surface Tension and Aggregate Formation Using Molecular Dynamics Simulations. *Atmos. Chem. Phys.* **2011**, *11*, 6549−6557.

(23) Li, X.; Hede, T.; Tu, Y.; Leck, C.; Ågren, H. Surface-Active cis-Pinonic Acid in Atmospheric Droplets: A Molecular Dynamics Study. *J. Phys. Chem. Lett.* **2010**, *1*, 769−773.

(24) Ma, X.; Chakraborty, P.; Henz, B. J.; Zachariah, M. R. Molecular Dynamic Simulation of Dicarboxylic Acid Coated Aqueous Aerosol: Structure and Processing of Water Vapor. *Phys. Chem. Chem. Phys.* **2011**, *13*, 9374−9384.

(25) Vacha, R.; Jungwirth, P.; Chen, J.; Valsaraj, K. T. Adsorption of Polycyclic Aromatic Hydrocarbons at the Air-Water Interface: Molecular Dynamics Simulations and Experimental Atmospheric Observations. *Phys. Chem. Chem. Phys.* **2006**, *8*, 4461−4467.

(26) Liyana-Arachchi, T. P.; Valsaraj, K. T.; Hung, F. R. Molecular Simulation Study of the Adsorption of Naphthalene and Ozone on Atmospheric Air/Ice Interfaces. *J. Phys. Chem. A* **2011**, *115*, 9226−9236.

(27) Hede, T.; Leck, C.; Sun, L.; Tu, Y.; Ågren, H. A Theoretical Study Revealing the Promotion of Light-Absorbing Carbon Particles Solubilization by Natural Surfactants in Nanosized Water Droplets. *Atmos. Sci. Lett.* **2013**, *14*, 86−90.

(28) Vacha, R.; Slavicek, P.; Mucha, M.; Finlayson-Pitts, B. J.; Jungwirth, P. Adsorption of Atmospherically Relevant Gases at the Air/Water Interface: Free Energy Profiles of Aqueous Solvation of N_2,

O_2, O_3, OH, H_2O, HO_2, and H_2O_2. *J. Phys. Chem. A* **2004**, *108*, 11573−11579.
(29) Wick, C. D.; Chen, B.; Valsaraj, K. T. Computational Investigation of the Influence of Surfactants on the Air-Water Interfacial Behavior of Polycylic Aromatic Hydrocarbons. *J. Phys. Chem. C* **2010**, *114*, 14520−14527.
(30) Vieceli, J.; Roeselova, M.; Potter, N.; Dang, L. X.; Garrett, B. C.; Tobias, D. J. Molecular Dynamics Simulations of Atmospheric Oxidants at the Air-Water Interface: Solvation and Accommodation of OH and O_3. *J. Phys. Chem. B* **2005**, *109*, 15876−15892.
(31) Roeselova, M.; Vieceli, J.; Dang, L. X.; Garrett, B. C.; Tobias, D. J. Hydroxyl Radical at the Air-Water Interface. *J. Am. Chem. Soc.* **2004**, *126*, 16308−16309.
(32) Harper, K.; Minofar, B.; Sierra-Hernandez, M. R.; Casillas-Ituarte, N. N.; Roeselova, M.; Allen, H. C. Surface Residence and Uptake of Methyl Chloride and Methyl Alcohol at the Air/Water Interface Studied by Vibrational Sum Frequency Spectroscopy and Molecular Dynamics. *J. Phys. Chem. A* **2009**, *113*, 2015−2024.
(33) Pasalic, H.; Roeselova, M.; Lischka, H. Methyl and Pentyl Chloride in a Microhydrated Environment and at the Liquid Water-Vapor Interface: A Theoretical Study. *J. Phys. Chem. B* **2011**, *115*, 1807−1816.
(34) Blando, J. D.; Turpin, B. J. Secondary Organic Aerosol Formation in Cloud and Fog Droplets: A Literature Evaluation of Plausibility. *Atmos. Environ.* **2000**, *34*, 1623−1632.
(35) Sander, R. *Compilation of Henry's Law Constants for Inorganic and Organic Species of Potential Importance in Environmental Chemistry*, Version 3, 1999; http://www.henrys-law.org (accessed September 9, 2011).
(36) Lemkul, J. A.; Bevan, D. R. Assessing the Stability of Alzheimer's Amyloid Protofibrils Using Molecular Dynamics. *J. Phys. Chem. B* **2010**, *114*, 1652−1660.
(37) Jagoda-Cwiklik, B.; Cwiklik, L.; Jungwirth, P. Behavior of the Eigen Form of Hydronium at the Air/Water Interface. *J. Phys. Chem. A* **2011**, *115*, 5881−5886.
(38) Hub, J. S.; de Groot, B. L.; van der Spoel, D. g_wham - A Free Weighted Histogram Analysis Implementation Including Robust Error and Autocorrelation Estimates. *J. Chem. Theory Comput.* **2010**, *6*, 3713−3720.
(39) Kumar, S.; Bouzida, D.; Swendsen, R. H.; Kollman, P. A.; Rosenberg, J. M. The Weighted Histogram Analysis Method for Free-Energy Calculations on Biomolecules. 1. The Method. *J. Comput. Chem.* **1992**, *13*, 1011−1021.
(40) Kumar, S.; Rosenberg, J. M.; Bouzida, D.; Swendsen, R. H.; Kollman, P. A. Multidimensional Free-Energy Calculations Using the Weighted Histogram Analysis Method. *J. Comput. Chem.* **1995**, *16*, 1339−1350.
(41) Hess, B.; Kutzner, C.; van der Spoel, D.; Lindahl, E. GROMACS 4: Algorithms for Highly Efficient, Load-Balanced, and Scalable Molecular Simulation. *J. Chem. Theory Comput.* **2008**, *4*, 435−447.
(42) Abascal, J. L. F.; Vega, C. A general purpose model for the condensed phases of water: TIP4P/2005. *J. Chem. Phys.* **2005**, *123*, 234505.
(43) Vega, C.; Abascal, J. L. F. Simulating Water with Rigid Non-Polarizable Models: A General Perspective. *Phys. Chem. Chem. Phys.* **2011**, *13*, 19663−19688.
(44) Vega, C.; Abascal, J. L. F.; Conde, M. M.; Aragones, J. L. What Ice Can Teach Us About Water Interactions: A Critical Comparison of the Performance of Different Water Models. *Faraday Discuss.* **2009**, *141*, 251−276.
(45) Wang, J.; Wolf, R. M.; Caldwell, J. W.; Kollman, P. A.; Case, D. A. Development and Testing of a General Amber Force Field. *J. Comput. Chem.* **2004**, *25*, 1157−1174.
(46) Bayly, C. I.; Cieplak, P.; Cornell, W. D.; Kollman, P. A. A Well-Behaved Electrostatic Potential Based Method Using Charge Restraints for Deriving Atomic Charges - the RESP Model. *J. Phys. Chem.* **1993**, *97*, 10269−10280.
(47) Frisch, M. J.; Trucks, G. W.; Schlegel, H. B.; Scuseria, G. E.; Robb, M. A.; Cheeseman, J. R.; Scalmani, G.; Barone, V.; Mennucci, B.; Petersson, G. A.; et al. *Gaussian 09, Revision A.1*; Gaussian, Inc.: Wallingford, CT, 2009.
(48) Case, D. A.; Darden, T. A.; Cheatham, T. E.; Simmerling, C. L.; Wang, J.; Duke, R. E.; Luo, R.; Merz, K. M.; Pearlman, D. A.; Crowley, M.; et al. *AMBER 9*; University of California: San Fransisco, 2006.
(49) Hockney, R. W.; Goel, S. P.; Eastwood, J. W. Quiet High-Resolution Computer Models of a Plasma. *J. Comput. Phys.* **1974**, *14*, 148−158.
(50) Bussi, G.; Donadio, D.; Parrinello, M. Canonical Sampling through Velocity Rescaling. *J. Chem. Phys.* **2007**, *126*, 014101.
(51) Darden, T.; York, D.; Pedersen, L. Particle Mesh Ewald - an N.Log(N) Method for Ewald Sums in Large Systems. *J. Chem. Phys.* **1993**, *98*, 10089−10092.
(52) Essmann, U.; Perera, L.; Berkowitz, M. L.; Darden, T.; Lee, H.; Pedersen, L. G. A Smooth Particle Mesh Ewald Method. *J. Chem. Phys.* **1995**, *103*, 8577−8593.
(53) Hess, B.; Bekker, H.; Berendsen, H. J. C.; Fraaije, J. Lincs: A Linear Constraint Solver for Molecular Simulations. *J. Comput. Chem.* **1997**, *18*, 1463−1472.
(54) Hub, J. S.; Caleman, C.; van der Spoel, D. Organic Molecules on the Surface of Water Droplets − an Energetic Perspective. *Phys. Chem. Chem. Phys.* **2012**, *14*, 9537−9545.
(55) Feller, D. The Role of Databases in Support of Computational Chemistry Calculations. *J. Comput. Chem.* **1996**, *17*, 1571−1586.
(56) Caleman, C.; Hub, J. S.; van Maaren, P. J.; van der Spoel, D. Atomistic Simulation of Ion Solvation in Water Explains Surface Preference of Halides. *Proc. Natl. Acad. Sci. U.S.A.* **2011**, *108*, 6838−6842.
(57) Zierkiewicz, W.; Michalska, D.; Havlas, Z.; Hobza, P. Study of the Nature of Improper Blue-Shifting Hydrogen Bonding and Standard Hydrogen Bonding in the $X_3CH—OH_2$ and $XH—OH_2$ Complexes (X = F, Cl, Br, I): A Correlated Ab Initio Study. *ChemPhysChem* **2002**, *3*, 511−518.
(58) Zhao, X.; Pang, X.; Yan, X.; Jin, W. Halogen Bonding or Hydrogen Bonding between 2,2,6,6-Tetramethyl-Piperidine-Noxyl Radical and Trihalomethanes CHX_3 (X = Cl, Br, I). *Chin. J. Chem. Phys.* **2013**, *26*, 172−180.
(59) Smith, J. S.; Valsaraj, K. T.; Thibodeaux, L. J. Bubble Column Reactors for Wastewater Treatment. 1. Theory and Modeling of Continuous Countercurrent Solvent Sublation. *Ind. Eng. Chem. Res.* **1996**, *35*, 1688−1699.
(60) Smith, J. S.; Burns, L. F.; Valsaraj, K. T.; Thibodeaux, L. J. Bubble Column Reactors for Wastewater Treatment. 2. The Effect of Sparger Design on Sublation Column Hydrodynamics in the Homogeneous Flow Regime. *Ind. Eng. Chem. Res.* **1996**, *35*, 1700−1710.
(61) Smith, J. S.; Valsaraj, K. T. Bubble Column Reactors for Wastewater Treatment. 3. Pilot-Scale Solvent Sublation of Pyrene and Pentachlorophenol from Simulated Wastewater. *Ind. Eng. Chem. Res.* **1997**, *36*, 903−914.
(62) Valsaraj, K. T. Trace gas adsorption thermodynamics at the air-water interface: Implications in atmospheric chemistry. *Pure Appl. Chem.* **2009**, *81*, 1889−1901.
(63) Nissenson, P.; Knox, C. J. H.; Finlayson-Pitts, B. J.; Phillips, L. F.; Dabdub, D. Enhanced Photolysis in Aerosols: Evidence for Important Surface Effects. *Phys. Chem. Chem. Phys.* **2006**, *8*, 4700−4710.
(64) Watanabe, H.; Yamaguchi, S.; Sen, S.; Morita, A.; Tahara, T. "Half-Hydration" at the Air/Water Interface Revealed by Heterodyne-Detected Electronic Sum Frequency Generation Spectroscopy, Polarization Second Harmonic Generation, and Molecular Dynamics Simulation. *J. Chem. Phys.* **2010**, *132*, 144701.